

Use of Global Satellite Altimeter and Drifter Data for Ocean Current Resource Characterization

Ruo-Shan Tseng, Yu-Chia Chang and Peter C. Chu

Introduction

Interest in renewable and green energy around the world is burgeoning, especially in countries that have very limited natural resources. Concerns about the depletion of fossil fuel sources, environmental pollution, and climate change are primary motivations in the quest for affordable energy alternatives that have less of a negative impact on the ecosystem than the conventional fossil fuel power plants. The Intergovernmental Panel on Climate Change has identified six alternative energy sources that have promising global potential: bioenergy, direct solar energy, geothermal energy, hydropower, wind energy, and ocean energy (Edenhofer and Kalkuhl 2011). Ocean energy involves a variety of technologies used to extract energy from sources such as waves, tidal streams, ocean currents, ocean thermal energy conversion, and salinity gradients. Although still in the early stages of development, ocean current energy can provide reliable and predictable power and base load supply. This chapter is focused on the characterization of ocean current power generation in the global oceans, particularly in the Pacific Ocean.

Ocean current energy usually refers to the kinetic energy contained in large-scale, open-ocean, near-surface currents. These ocean currents are generally persistent, sustainable, much faster than background ocean currents and exhibit the strongest flows near the ocean surface. Using ocean currents to drive turbines and

R.-S. Tseng (✉)
Department of Oceanography, National Sun Yat-sen University,
Kaohsiung, Taiwan
e-mail: rstseng@mail.nsysu.edu.tw

Y.-C. Chang
Department of Marine Biotechnology and Resources,
National Sun Yat-sen University, Kaohsiung, Taiwan

P.C. Chu
Department of Oceanography, Naval Postgraduate School, Monterey, USA

generate electricity has been studied over the past several decades (Lissaman 1979; Hanson et al. 2010; Duerr and Dhanak 2012; Yang et al. 2014). VanZwieten et al. (2013) provide an initial assessment of kinetic energy flux in the worldwide ocean current systems based on three years (2009–2011) of HYbrid Coordinate Ocean Model (HYCOM) data. Eight regions with time-averaged power densities of at least 500 W/m^2 were compared and discussed along with other factors such as the variability of power density, distances from land, and areas of sea surface with selected average power densities. VanZwieten et al. (2014) further expanded the analysis based on a longer time series of HYCOM data and included current direction variability. Studies to characterize region-specific ocean current resources have been performed for some western boundary currents of the Pacific and Atlantic oceans, especially in the Florida Current of the Gulf Stream system in the USA (Duerr and Dhanak 2012; Yang et al. 2014, 2015a), the Kuroshio Current near Taiwan and Japan (Chen 2010; Chang et al. 2015), and the Agulhas Current off the coast of South Africa (Bryden et al. 2005; Lutjeharms 2006). Duerr and Dhanak (2012) estimate that approximately 25 GW of hydrokinetic power is available in the Florida Current, while Yang et al. (2014) have shown that the average power dissipated ranges between 4 and 6 GW, when considering extraction over a region composed of the Florida Current portion of the Gulf Stream system.

Previous studies that assessed the energy production potential of ocean currents were mostly based on available ocean model data such as the HYCOM, Navy Coastal Ocean Model (NCOM), Regional Ocean Modeling System (ROMS), and in situ-measured data such as those derived from moored Acoustic Doppler Current Profilers (ADCPs). The output data from the archived Global HYCOM normally have a temporal resolution of 1 day and a spatial resolution of 1–7 km, which is insufficient for the prediction of the core location and temporal variability of strong currents. Comparison of HYCOM with in situ ADCP data in two regions, the Florida Strait and the Agulhas Current off the coast of South Africa, indicates that the variability of current speed and the mean current speed was both underpredicted by HYCOM (VanZwieten et al. 2014). This underprediction may result in underestimation of the available power. Despite the lack of exact correlation with measurements, HYCOM still appears to be a useful tool for preliminary identification of areas in which to develop ocean current energy. On the other hand, Chang et al. (2015) employed a different and novel method. They analyzed the historical drifter data set to estimate the mean current and occurrence frequency in $0.25^\circ \times 0.25^\circ$ bins and used this information to select sites for the development of potential ocean current power generation. Due to its accumulated large amount of data over the past several decades and the Lagrangian perspective of flow measurement with drifters drogued at 15 m depth, Chang et al.'s (2015) method provides another interesting view of ocean current characterization. Still another method of observing ocean surface geostrophic current is to use the satellite altimeter. Chang et al. (2013) employed satellite altimeter data for ship navigational use.

Building upon data derived from historical drifters, satellite altimeters, and scatterometers, previous studies have used statistics to determine the flow patterns of global surface currents and mean streamlines (Niiler 2001; Chu 2009;

Maximenko et al. 2009; Lumpkin and Johnson 2013). Knowledge of global surface currents can be used in current power generation, rescue efforts, oil spill response, and ship routing (Ponta and Jacovkis 2008; Davidson et al. 2009; Chang et al. 2013). Strong ocean currents often occur during tropical cyclones or high-wind-speed conditions (Chang et al. 2010, 2012, 2014). A distinct feature of ocean circulation that is driven by surface winds is the so-called intensification of western boundary currents (WBCs). WBCs are formed by the momentum balance of the wind stress, friction, and increase in the Coriolis parameter with latitude. Based on the conservation of mass and potential vorticity, earlier studies (Stommel 1948; Munk 1950) indicated that the WBCs of the subtropical gyre are narrow, strong ocean currents along the western boundaries of the world's major ocean basins. In the WBC regions that have extremely strong flow, such as the Kuroshio Current, ocean currents can potentially provide sufficient, renewable, clean, and possibly cost-effective power.

The purpose of this chapter is to characterize global ocean current resources by analyzing in situ ocean current data from surface drifters and satellite altimeters; provide a complete map of strong currents that have high power densities; and identify possible sites for ocean current power plants in the world's oceans, emphasizing the Pacific Ocean and neighboring marginal seas. The data and analysis method used is described in section “[Data and Method](#)”. The distribution of the strong ocean currents and their temporal and spatial variations in the global oceans are discussed in section “[Strong Ocean Currents and the Seasonal Variation of Current Speeds](#)”. The potential sites for ocean current power generation—determined using a criterion that combines several factors, including location and current speed—are given in section “[Ocean Current Power Resource](#)”, followed by a discussion, summary, and concluding remarks.

Data and Method

In this study, the surface geostrophic currents of 1992–2012, derived from a merged product of ocean Topography Experiment/Poseidon, Jason 1, and European Research Satellite altimeter observations, are used to examine the circulation of the global ocean surface. Produced by the French Archiving, Validation, and Interpolation of Satellite Oceanographic Data (AVISO) project using the mapping method of Ducet et al. (2000), the absolute geostrophic currents can be obtained from the AVISO Web site (<http://aviso.altimetry.fr/index.php?id=1271>). The optimal interpolation with realistic correlation functions generates a combined map merging measurements from all available altimeter missions (Ducet et al. 2000) to greatly improve the estimation of mesoscale signals. The data are interpolated onto a global grid of $1/3^\circ$ resolution between 82° S and 82° N and are archived in weekly (7-day) averaged frames. The geostrophic currents are calculated from the absolute dynamic topography (ADT), which consists of a mean dynamic topography and the sea-level anomalies. Rio and Hernandez (2004) have explained in detail the method of estimating the ADT.

The resulting geostrophic currents have been validated by independent drifter data with a root-mean-square difference of about 14 cm/s in the area of the Kuroshio Current (Rio and Hernandez 2004). Readers are referred to Le Traon et al. (2001) and Pascual et al. (2006) for more details on the data analysis method.

Direct velocity measurements in the mixed layer of the ocean are obtained using satellite-tracked Surface Velocity Program (SVP) drifters drogued at a nominal depth of 15 m to reduce the downwind slip. Drifter data are acquired from an enhanced version of the global drifter data set maintained at Atlantic Oceanographic and Meteorological Laboratory, available online at (<http://www.aoml.noaa.gov/phod/dac/dacdata.html>) (Niiler 2001). Drifter positions are determined every few hours, depending on latitudes, by Doppler ranging with the Argos satellite system. Time series of irregular drifter positions are interpolated to a 6-h interval by Kriging. The estimated accuracy of the velocity measurements in a 10 ms^{-1} wind is 10^{-2} ms^{-1} when the drogue remains attached to the drifter (Niiler et al. 1995). If the drogue is lost, the downwind slip increases to 1–1.5% of the wind speed (Poulain et al. 2009). We only use drogued drifter data collected from 1979 to 2012 in this study.

Data acquired from six high-frequency (HF) radar stations along the east coast of Taiwan over a three-year period (2013–2015) were used to map the sea surface currents and the Kuroshio Current east of Taiwan. These radar stations are operated by the Taiwan Ocean Research Institute. Each station is equipped with a coastal ocean dynamic application radar, long-ranger model, with a practical spatial observation radius of up to 220 km and a horizontal resolution of around 8 km in the radial direction and 2° in azimuth. Detailed analysis of signal processing and noise removal to obtain the sea surface currents can be found in Yang et al. (2015b).

Strong Ocean Currents and the Seasonal Variation of Current Speeds

Maps of the mean absolute geostrophic surface current speeds in the global oceans based on analysis of 21 years of AVISO data averaged in $1/3^\circ \times 1/3^\circ$ bins (Fig. 1) clearly show the subtropical gyre in the Northern Hemisphere associated with the intensification of WBCs. Note that all WBCs feature maximum current speeds in excess of 0.6 ms^{-1} can be clearly identified in each major ocean basin. These WBCs are the South Equatorial Current (SEC), Gulf Stream (GS), North Brazil Current, and Brazil Current of the Atlantic Ocean; the SEC, North Equatorial Counter Current, Kuroshio Current (KC), Mindanao Current (MC), and East Australian Current of the Pacific Ocean; and the Agulhas Current (AC), Mozambique Current, and Antarctic Circumpolar Current of the Indian Ocean. Hsin et al. (2013) used mean shipboard-ADCP (Sb-ADCP)-derived depth-averaged current (0–150 m) between 1991 and 2005 to verify AVISO absolute geostrophic velocity at the region of the KC east of Taiwan. Their results indicated that the mean AVISO

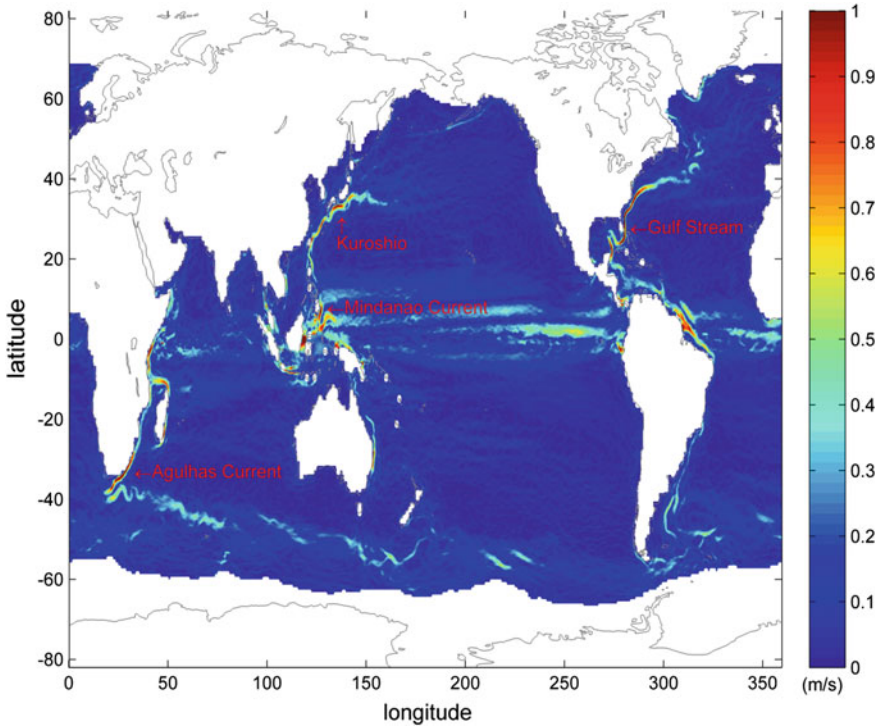


Fig. 1 Averaged near-surface geostrophic current speeds in $1/3^\circ \times 1/3^\circ$ bins of the world oceans from the AVISO satellite altimeter data of 1992–2012

absolute geostrophic velocities are smaller than the mean velocities derived using the Sb-ADCP, but the overall flow pattern of the KC is similar.

Historical SVP drifter data from 1979 to 2012 (34 years) were also processed by the ensemble average method (Centurioni et al. 2004) in $1/3^\circ \times 1/3^\circ$ bins to display the mean near-surface current field of the world oceans, as shown in Fig. 2. The number of independent observations of SVP drifters is shown in Fig. 3. More drifter data can be found in the eastern, western boundaries, and the equatorial waters of the North Pacific Ocean as well as the North Atlantic Ocean. Overall, drifter data about the world oceans are sufficient, which greatly improves the quality of our estimates. A comparison between Figs. 1 and 2 finds mostly similar features, further supporting the well-known results for global upper-ocean circulation as well as the location and speed of the strong flows derived from two independent data sets. Note that the 6-h drifter-measured data can reveal details of small length scale (e.g., small-scale eddy) and short timescale (e.g., tidal current) components of ocean currents, and the weekly averaged altimeter-observed data can yield underestimation of maximum currents and smooth out spatial and temporal variabilities. Also note that the drifter-measured velocity at the 15 m depth might be somewhat different than satellite-measured absolute geostrophic velocity at the sea surface.

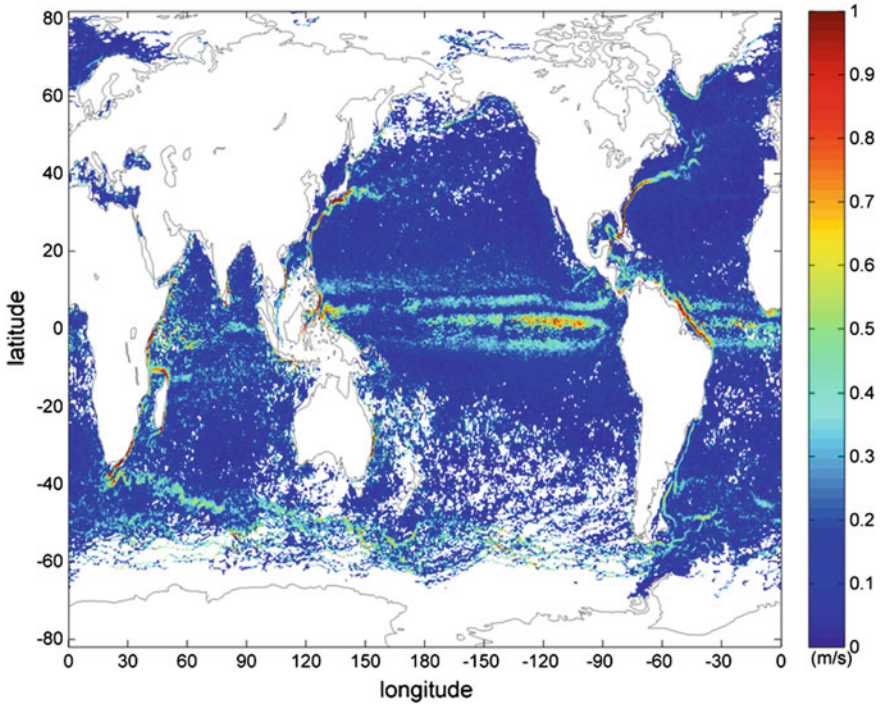


Fig. 2 Averaged near-surface current speeds in $1/3^\circ \times 1/3^\circ$ bins of the world oceans from the global drifter climatology of 1979–2012

A comparison between the drifter-observed current velocities and HF radar-mapped surface current velocities east of Taiwan averaged over three years (2013–2015) was also conducted during this study. Our results (not depicted here) show that the flow patterns of the KC in this region derived from the two data sets are similar. However, the drifter-observed currents are slightly higher than the HF radar-mapped currents.

Among the global ocean currents, the four WBCs that are most prominent have a 21-year mean speed (1992–2012) at a certain grid point ($1/3^\circ \times 1/3^\circ$) greater than 1 ms^{-1} , as can be clearly seen from both satellite altimeter and drifter observations. These four fast currents are the AC (Indian Ocean), GS (Atlantic Ocean), MC (Pacific Ocean), and KC (Pacific Ocean). Figures 4 and 5 show the enlarged plots of these four WBCs derived from satellite altimeter and drifter observations, respectively. The maximum of the mean surface speeds of the AC, GS, MC, and KC based on altimeter data are 1.41 , 1.32 , 1.12 , and 1.01 ms^{-1} , respectively. The locations of maximum speeds for the AC, GS, MC, and KC are near Port Elizabeth in South Africa (26.3° E , 34.5° S), Miami in the USA (79.7° W , 26.9° N), Caraga in the Philippines (126.7° E , 6.6° N), and Higashimuro in Japan (134.7° E , 33.9° N), respectively, as shown in the magenta triangles in Fig. 4. Bryden et al.

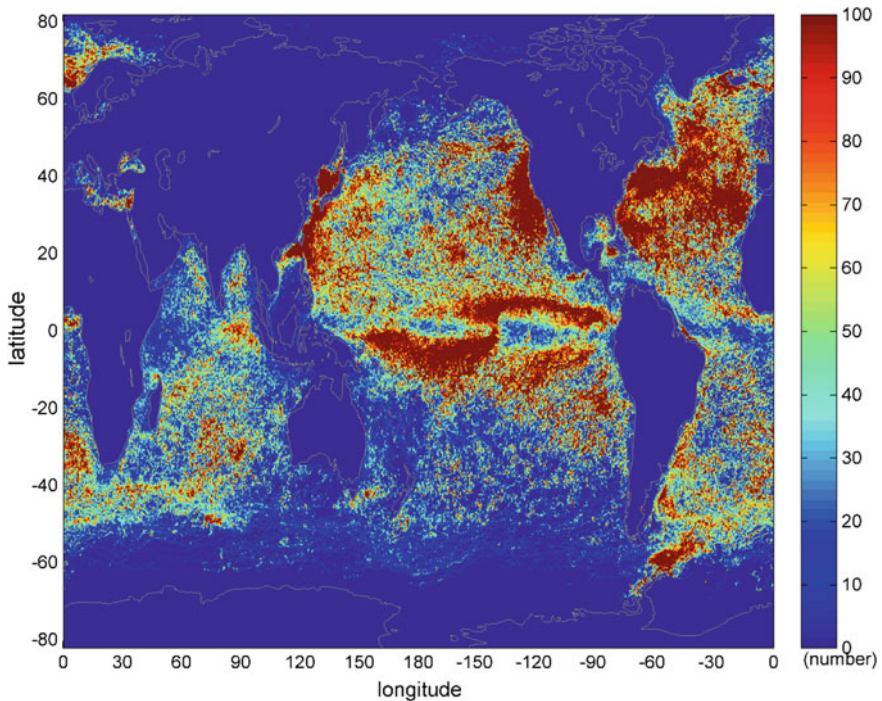


Fig. 3 Numbers of drifter data point in $1/3^\circ \times 1/3^\circ$ bins

(2005) indicated that the transport of the AC is larger than that of either the GS or KC at comparable latitudes ($24\text{--}32^\circ$ N and $24\text{--}32^\circ$ S). The net transports of the AC, GS, MC, and KC are estimated to be 70, 30, 33, and 22 Sv ($1 \text{ Sv} = 10^6 \text{ m}^3 \text{ s}^{-1}$) at 31° S, 27° N, 5.5° N, and 24° N, respectively (Lukas et al. 1991; Stramma and Lutjeharms 1997; Johns et al. 2001; Bryden et al. 2005). The present study shows that the AC, with a maximum of mean surface speed of 1.4 ms^{-1} , is stronger than the GS (1.3 ms^{-1}) and KC (1.0 ms^{-1}), which suggests that the AC is the strongest WBC in the world oceans in terms of maximum current speeds and volume transport.

Monthly averaged surface geostrophic current speeds and the number of data points from satellite altimeter measurements for the AC, GS, KC, and MC at the respective locations of their maximum current speeds are plotted in Fig. 6. Except for the MC, which is at around 5.5° N, the other three WBCs all show clear seasonal variations with higher current speeds occurring in the summer (August for the GS and KC in the Northern Hemisphere and February for the AC in the Southern Hemisphere) and lower speeds occurring in the winter. In terms of mean maximum current speeds, the AC is the strongest WBC, followed by the GS, MC, and KC. Note that the KC and AC have more marked interannual variations, which are represented by the larger error bars in Fig. 6.

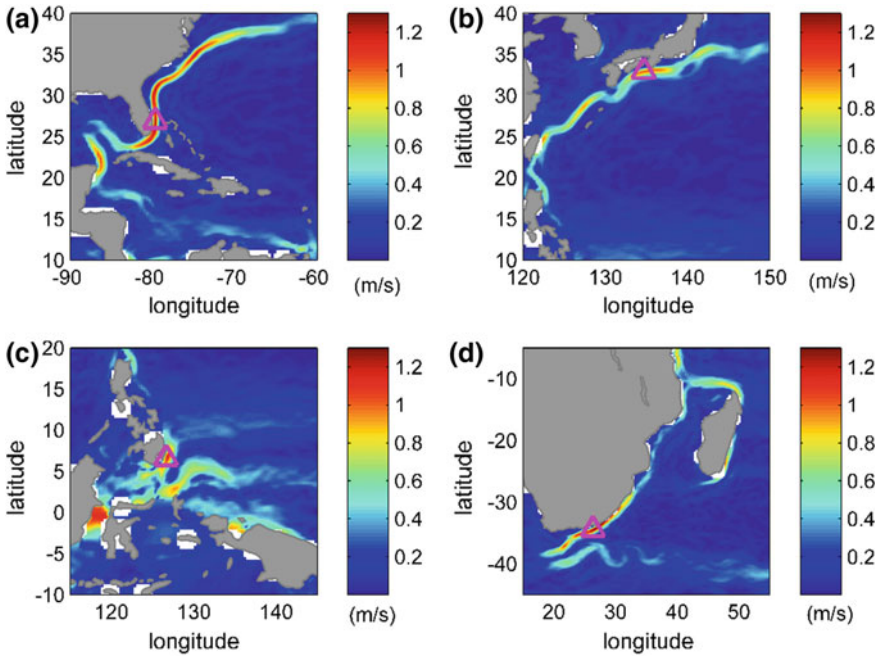


Fig. 4 The four WBCs of the **a** Gulf Stream, **b** Kuroshio Current, **c** Mindanao Current, and **d** Agulhas Current from the AVISO satellite altimeter data. The *magenta triangles* marked in each panel are locations of maximum current speeds and are used in Fig. 6

The mechanisms that cause the variability of the velocity and transport of WBCs have been studied by a number of researchers. For instance, Johns et al. (2001) showed that the instantaneous maximum surface velocities of the KC reach extreme values of 2.0 ms^{-1} and typical values of 1.5 ms^{-1} , based on data derived from a moored current meter array off northeastern Taiwan. On seasonal timescales, Hsin et al. (2013) indicated that the KC off the eastern coast of Taiwan tends to migrate inshore and have a smaller volume transport in winter and to shift offshore and have a larger transport in summer. Results from recent, intensive three-year observations off eastern Taiwan by multiple platforms (Sb-ADCP, Seagliders, SVP drifters, HF radars, and numerical models) reveal new insights into the mean structure and variability of the KC (Yang et al. 2015b). On the interannual timescale, the KC has a weaker volume transport during El Niño years (Kashino et al. 2009; Qiu and Chen 2006).

Ocean Current Power Resource

To curb global warming, many developed countries have devoted large efforts to reducing greenhouse gas emissions and developing devices to harness renewable energy. A 2006 report from the US Department of the Interior indicated that the

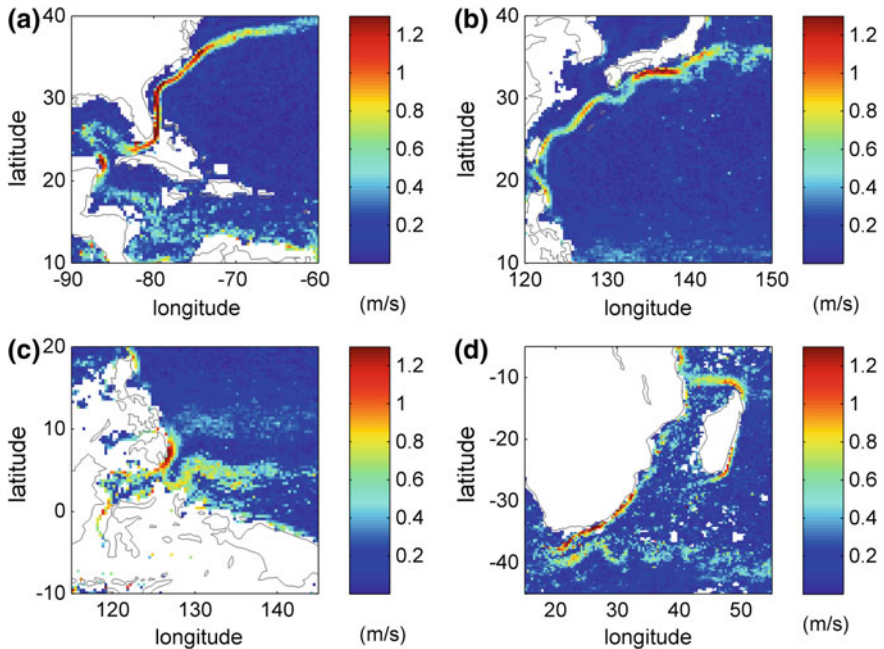


Fig. 5 The four WCBs of the **a** Gulf Stream, **b** Kuroshio Current, **c** Mindanao Current, and **d** Agulhas Current from the drifter climatology. A comparison between Figs. 4 and 5 finds mostly similar features, further supporting the location of the strong flows derived from two independent data sets

total worldwide power contained in ocean currents has been estimated to be about 5,000 GW (<http://www.e-renewables.com/documents/Ocean/Ocean%20Current%20Energy%20Potential.pdf>). The ocean current power P_o (Wm^{-2}) from a generator is given by (Twidell and Weir 2006; Bahaj 2011):

$$P_o = \frac{1}{2} \rho A U^3 \tag{1}$$

where ρ is the density of seawater ($\sim 1023 \text{ kg m}^{-3}$), A is the cross-sectional area of the rotor under consideration, and U is the ocean current speed. Note that actual recoverable energy will be much lower than ocean current power P_o because of turbine and transmission efficiency, backwater effect, etc. Devices that extract power from a fluid’s momentum only can realistically reach an efficiency of about 50% (Chang et al. 2015). Figure 7 shows the average marine surface current power in the world oceans including the current speed obtained from satellite observations. The available power density from the four WCBs has values ranging from 500 to 1400 Wm^{-2} . Note that these values are based on mean surface current speed, so they only represent the power level at the surface. The power level throughout the water column will be smaller than these values, considering the typical velocity

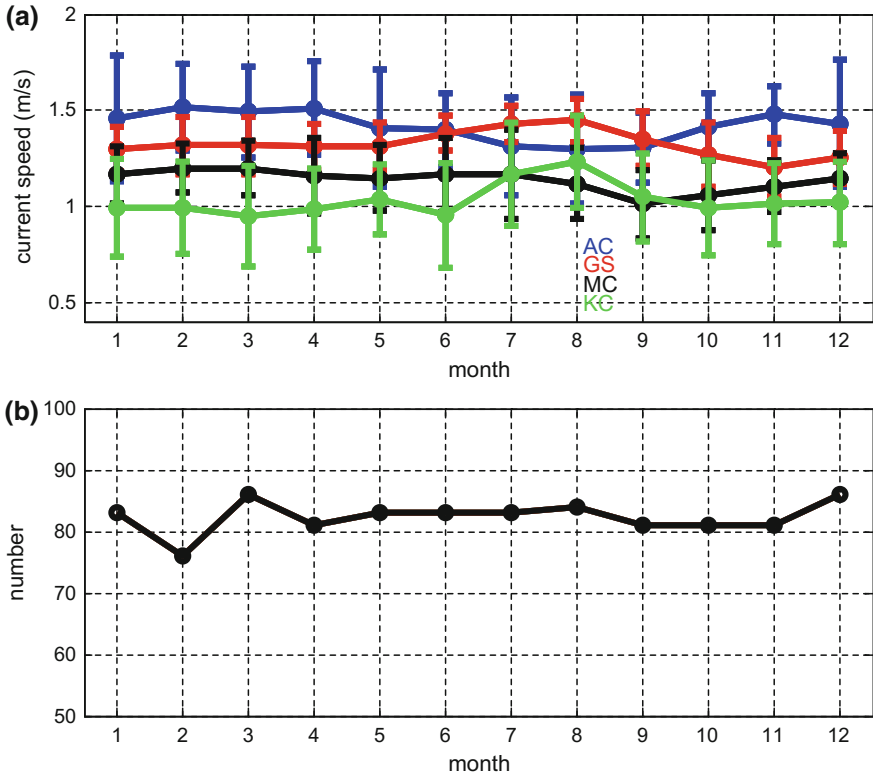


Fig. 6 **a** Monthly mean current speeds of the Agulhas Current, Gulf Stream, Mindanao Current, and Kuroshio Current from altimeter measurements at the locations marked as *magenta triangles* in Fig. 4. The *error bars* represent one standard deviation, and **b** is the monthly number of data points

profiles of decreasing velocities away from the sea surface. The largest current power of 1403 Wm^{-2} is found for the AC, and its core position (*magenta triangles*) is near Port Elizabeth, South Africa. This provides a global statement from a very limited location. Other estimated current power densities for the GS, MC, and KC are approximately 1124 , 681 , and 512 Wm^{-2} near Miami in the USA, Caraga in the Philippines, and Higashimuro in Japan, respectively. VanZwieten et al. (2013) also computed the time-averaged power density for various regions of the world oceans at a depth of 50 m based on three-year HYCOM results. Eight areas that might be minimally eligible for consideration of ocean current turbines' production sites were identified by VanZwieten et al. (2013), and each had a power density greater than 500 Wm^{-2} . Our results are largely consistent with those of VanZwieten et al.'s (2013), but ours show a more detailed distribution of power density in various regions. Note that current speed is not the only factor considered when determining suitable locations for power plants. Other factors, such as the

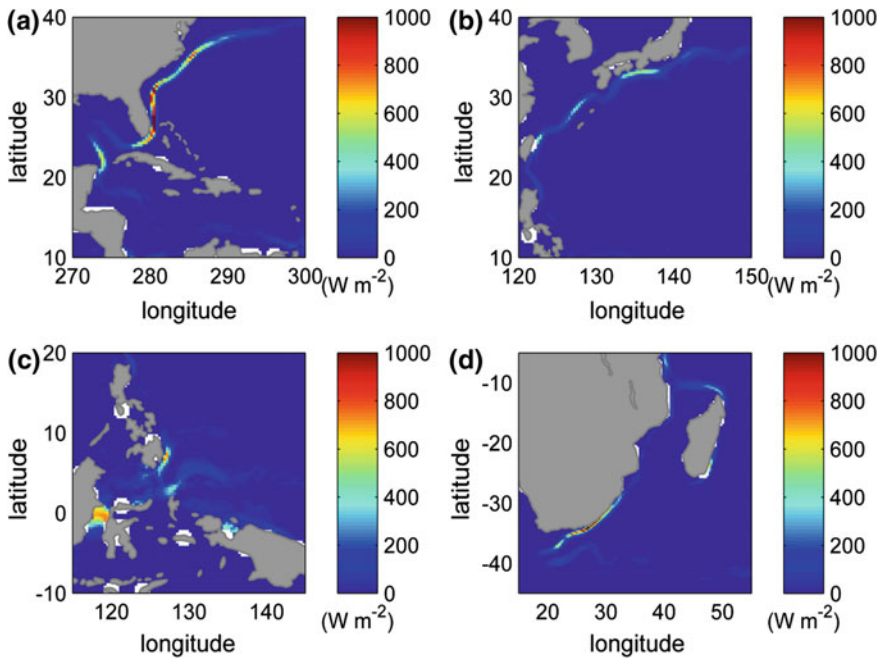


Fig. 7 Average ocean current power (W m^{-2}) of **a** Gulf Stream, **b** Kuroshio, **c** Mindanao Current, and **d** Agulhas Current from the AVISO satellite altimeter data

water depth, distance from the shore, and stability of currents, should also be considered. For instance, there are two modes of the KC path off southern Japan—the large meander path and the non-large meander path (Kawabe 2005). If turbine generators are to be set up near the coast, the speed of ocean current could become substantially weaker during the large meander path period.

Site Selection for Ocean Current Power Generation

Selection of a potential site for ocean current power generation can be achieved by considering various factors, such as the maximum average power density, distances from land, areas of sea surface with selected average power densities, depth of seafloor, and flow direction variability (VanZwieten et al. 2013, 2014). More recently, Chang et al. (2015) used an index I , which is based on four factors (distance to the coast, water depth, mean flow speed, and maximum flow speed), to determine potential sites for ocean current power generation. Using the mean current speed derived from a long, historical drifter data set (1985–2009), Chang et al. (2015) found several suitable sites in the strong ocean currents of the East Asia, i.e., the KC in the northwestern Pacific Ocean south of Japan, east of Taiwan,

and northeast of Luzon; and the coastal jets east of Vietnam in the South China Sea. In this chapter, we use the same index I , but a different data set of surface geostrophic currents derived from satellite altimeters, to find some potential sites for ocean current power generation. A comparison between the analyzed results from the two different data sets is made and discussed.

Index I is expressed as the summation of four subindices, I_i , multiplied by each of their respective weights, W_i (Chang et al. 2015), i.e.,

$$I = \sum_{i=1}^4 W_i I_i, \quad (2)$$

where $I_1 = [1 - (L/50 \text{ km})]$, $I_2 = [1 - (D/1000 \text{ m})]$, $I_3 = P$, and $I_4 = U/1.4 \text{ ms}^{-1}$. Here, L is the shortest distance to a power station; D is the water depth; P is the percentage of current speed greater than 1 ms^{-1} ; and U is the current speed. The choice of constants ($L = 50 \text{ km}$, $D = 1000 \text{ m}$, and $U = 1.4 \text{ ms}^{-1}$) is based on the results of several earlier studies (Finkl and Charlier 2009; Chen 2010; Chang et al. 2015). Each of these indices was weighted to reflect its impact on revenue, capital costs, maintenance costs, etc. According to the financial analysis of the capital cost, operational expenses, and sales income of a 30-MW pilot plant assuming a lifetime of 20 years, percentages of expenditure and income can be estimated to be 31% and 69%, respectively (Chen 2010; Chang et al. 2015). I_1 and I_2 reflect the impact on expenditure, while I_3 and I_4 reflect the impact on revenue. Assuming a 50/50 equivalent weighting, w_1 and w_2 are each set to be 15.5%, and w_3 and w_4 are each set to be 34.5% (Chang et al. 2015). Note that the results of site selection will be very dependent on the choice of the subindices and their respective weights. Some sort of sensitivity test will need to be performed on the chosen values for w_i in future research. In this study, we followed the same approach and analysis of Chang et al. (2015).

The depth (D) and the shortest distance from shore (L) for any point in the world oceans can be calculated from coastline data, which can be downloaded from the National Oceanic and Atmospheric Administration–National Geophysical Data Center Web site. With the available topographic data and the mean surface geostrophic current averaged from 21 years of AVISO data, the index I of the global oceans can be computed according to Eq. (2). Variations of the index I are shown in Figs. 8 and 9 for East Asia and Southeast Asia and Oceania, respectively. Note that the higher the index value is, the more suitable the site is for ocean current power generation. In East Asia, our results indicate that there are more ocean surface areas near the coast of Japan that have index values greater than 0.3, followed by the regions off the Philippines, Vietnam, Taiwan, South Korea, and China (Fig. 8). Some sites that have particularly high index values, ranging between 0.3 and 0.5, are within the KC south of Japan, the upstream KC northeast of Taiwan, the coastal jet off eastern Vietnam, and the upstream KC and MC off the Philippines.

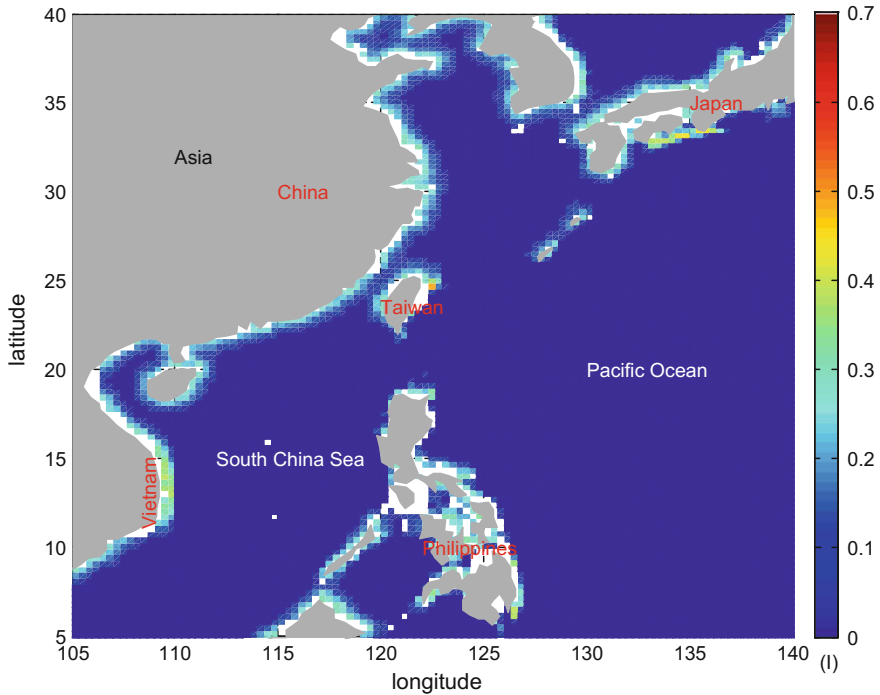


Fig. 8 Enlargement of index I and suitable ocean current power generation sites in East Asia

A comparison between the estimated index values, using mean surface currents from historical drifter data (Fig. 10) and using surface geostrophic currents from satellite altimeters (Fig. 8), shows mostly similar results. Figures 8 and 10 both suggest that the most suitable region to develop for ocean current power generation is the shallow coastal water near Japan, Taiwan, Vietnam, and the Philippines. Furthermore, the present results can reveal more detailed features of I and its spatial distribution because the AVISO surface geostrophic current data have more comprehensive coverage globally than the drifter data. For example, there are no or very few drifter data available for the coastal waters of the East China Sea and South China Sea. As the conditions of subindices become harsher, the number of sites selected becomes smaller (Fig. 11). Nevertheless, it should be noted that the AVISO weekly data on surface geostrophic currents may underestimate the current speed and thus the power potential. Figure 9 shows that in Southeast Asia and Oceania, more ocean surface areas near the coasts of Indonesia have the largest index values, ranging between 0.3 and 0.65, followed by Malaysia, Papua New Guinea, and Australia.

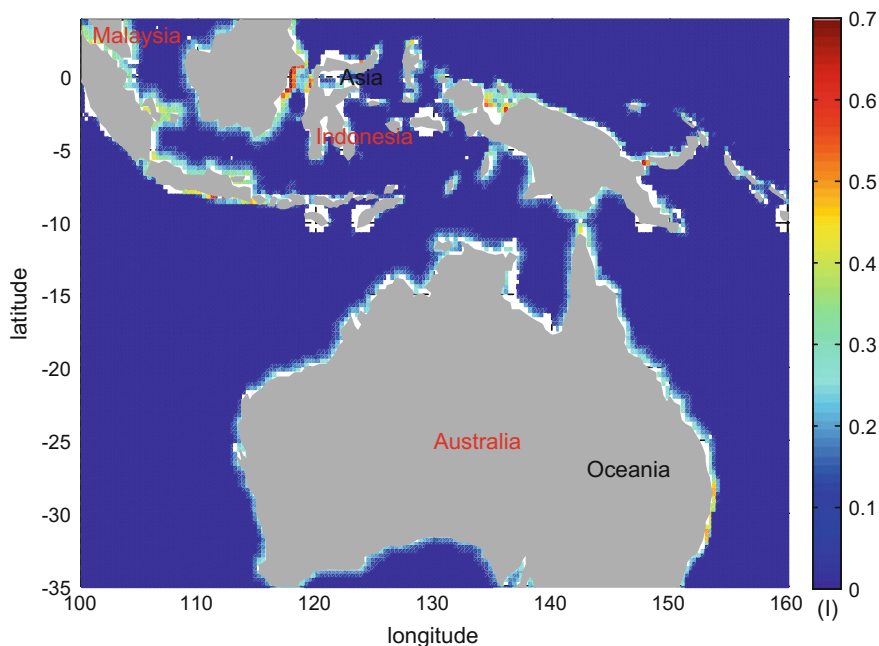


Fig. 9 Enlargement of index I and suitable ocean current power generation sites in Southeast Asia and Oceania

Discussion and Conclusions

This study has illustrated flow patterns of strong near-surface currents in the western boundaries of world oceans by analyzing two relatively long data sets of velocity measurements derived from satellite altimeters and SVP drifters. Current speeds in excess of 1.0 ms^{-1} were observed in the four strongest WBCs, and the 21-year averaged velocity maximums were 1.4, 1.3, 1.1, and 1.0 ms^{-1} for the AC, GS, MC, and KC, respectively. The locations of maximum velocities for these four WBCs are near Port Elizabeth in South Africa (26.3° E , 34.5° S), Miami in the USA (79.7° W , 26.9° N), Caraga in the Philippines (126.7° E , 6.6° N), and Higashimuro in Japan (134.7° E , 33.9° N), respectively. Temporal variability of the WBCs is significant at the seasonal timescale, which is influenced by the monsoon winds, and at the interannual timescale, which is connected to the El Niño–Southern Oscillation phenomenon.

The maximum available mean, undisturbed current power from these four WBCs is 1403, 1124, 681, and 512 Wm^{-2} , respectively, for the AC, GS, MC, and KC. Assessment of ocean current energy in previous studies was mostly based on numerical ocean calculation models (HYCOM, NCOM, JPL ROMS, etc.). In this study, the selection of sites for ocean current power generation in the Pacific Ocean and South China Sea is done by calculating the index values in each grid. Doing so

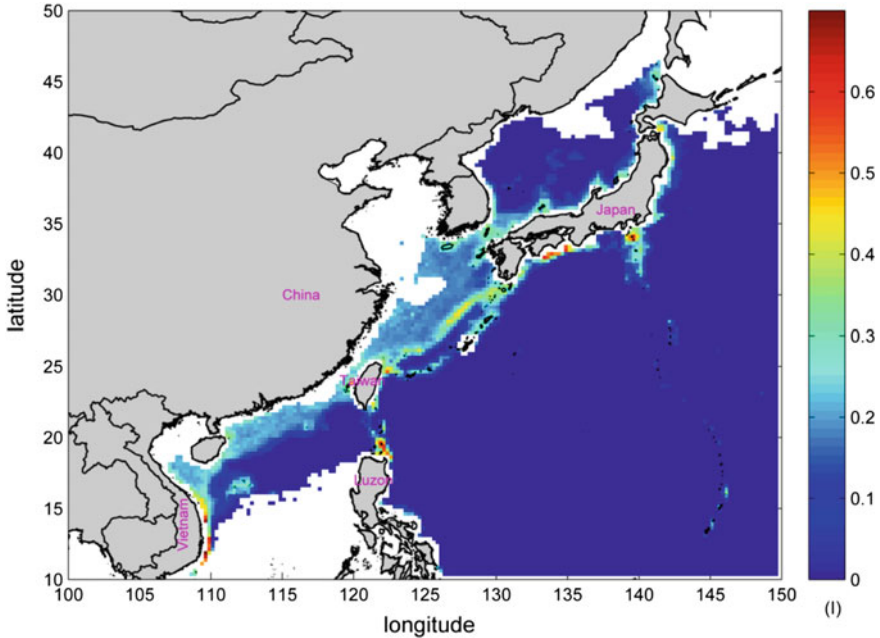


Fig. 10 Distribution of index I in East Asia from drifter-derived mean surface current. *Reproduced from Chang et al. (2015)*

depends on four factors: the frequency with which currents occur, the magnitudes of their speed, the depth at which they occur, and their distance from the shore. In situ near-surface current data from SVP drifters and AVISO satellite altimeters are used. Our results indicate that Japan, Taiwan, Vietnam, the Philippines, Malaysia, Papua New Guinea, and Australia have promising potential for the development of ocean current power generation.

One factor we have ignored in the estimation of maximum available power is the backwater effect, including turbine and transmission efficiencies, losses from supporting structures, and wake interference. This is a practical issue of concern for ocean current power engineering design and has received attention recently (Garrett and Cummins 2007, 2008; Yang et al. 2013). Numerical modeling results from the recent studies indicate that the maximum extractable energy strongly depends on the turbine hub height in the water column, and there is a limit to the available power because too many turbines will merely block the flow. Further investigation is suggested to be pursued along this line.

Further analysis is also required relative to Eq. (2) for the index calculation. “ P ” and “ U ” in this equation are two interdependent parameters; a higher value of P will result in a higher value of U . Thus, more justification is needed to choose a best value. Some sort of sensitivity test relative to the values of the weights w_i will be performed in the future.

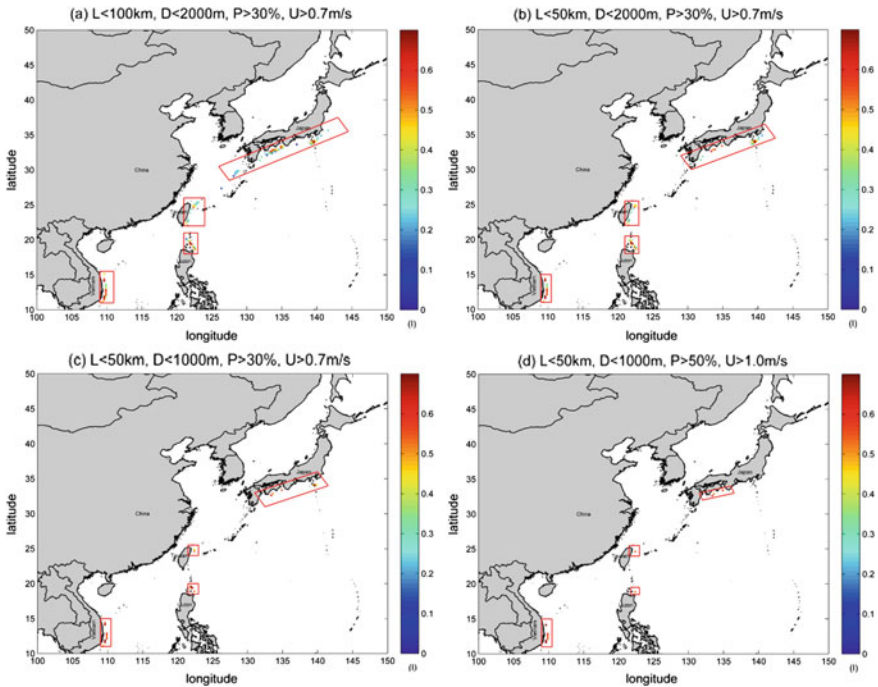


Fig. 11 Selected sites in conditions of **a** $L < 100$ km, $D < 2000$ m, $P > 30\%$, and $U > 0.7$ ms^{-1} ; **b** $L < 50$ km, $D < 2000$ m, $P > 30\%$, and $U > 0.7$ ms^{-1} ; **c** $L < 50$ km, $D > 1000$ m, $P > 30\%$, and $U > 0.7$ ms^{-1} ; and **d** $L < 50$ km, $D < 1000$ m, $P > 50\%$, and $U > 1.0$ ms^{-1} . *Reproduced from Chang et al. (2015)*

Finally, other factors are potentially important and might need to be included in the index determination—factors such as sea state condition (rough vs. calm, this will have a huge impact on the engineering design and installation and maintenance cost), marine environment consideration (whether the sea area is a protected natural reserve), and socioeconomic factors (levelized cost of energy, which also depends on environmental concerns, permitting challenges, and comparisons between the cost of energy for non-renewable sources vs. renewable sources of power and timeline under consideration). These are some important tasks to be completed in the future.

Acknowledgements This research was completed with grants from the Ministry of Science and Technology of Taiwan, the Republic of China (MOST 104-2611-M-10-008). Peter C. Chu was supported by the Naval Oceanographic Office. We are grateful for the comments of anonymous reviewers. We thank Luca Centurioni of Scripps Institution of Oceanography for providing drifter data.

References

- Bahaj, A. S. (2011). Generating electricity from the oceans. *Renewable and Sustainable Energy Reviews*, *15*, 3399–3416.
- Bryden, H., Beal, L. M., & Duncan, L. M. (2005). Structure and Transport of the Agulhas current and its temporal variability. *Journal of Oceanography*, *61*, 479–492.
- Centurioni, L. R., Niller, P. P., & Lee, D.-K. (2004). Observations of inflow of Philippine sea surface water into the South China Sea through the Luzon Strait. *Journal of Physical Oceanography*, *34*, 113–121.
- Chang, Y.-C., Tseng, R.-S., & Centurioni, L. R. (2010). Typhoon-induced strong surface flows in the Taiwan Strait and Pacific. *Journal of Oceanography*, *66*, 175–182.
- Chang, Y.-C., Chen, G.-Y., Tseng, R.-S., Centurioni, L. R., & Chu, P. C. (2012). Observed near-surface currents under high wind speeds. *Journal Geophysical Research*, *117*, C11026. doi:10.1029/2012JC007996.
- Chang, Y.-C., Tseng, R.-S., Chen, G.-Y., Chu, P. C., & Shen, Y.-T. (2013). Ship routing utilizing strong ocean currents. *Journal of Navigation*, *66*, 825–835.
- Chang, Y.-C., Chu, P. C., Tseng, R.-S., & Centurioni, L. R. (2014). Observed near-surface currents under four super typhoons. *Journal of Marine Systems*, *139*, 311–319.
- Chang, Y.-C., Tseng, R.-S., & Chu, P. C. (2015). Site selection of ocean current power generation from drifter measurements. *Renewable Energy*, *80*, 737–745.
- Chen, F. (2010). Kuroshio power plant development plan. *Renewable and Sustainable Energy Reviews*, *14*, 2655–2668.
- Chu, P. C. (2009). Statistical characteristics of the global surface current speeds obtained from satellite altimeter and scatterometer data. *IEEE Journal of Selected Topics in Applied Earth Observations and Remote Sensing*, *2*(1), 27–32.
- Davidson, F. J. M., Allen, A., Brassington, G. B., Breivik, Ø, Daniel, P., Kamachi, M., et al. (2009). Applications of GODAE ocean current forecasts to search and rescue and ship routing. *Oceanography*, *22* (3), 176–181.
- Ducet, N., Le Traon, P.-Y., & Reverdin, G. (2000). Global high resolution mapping of ocean circulation from TOPEX/Poseidon and ERS-1 and -2. *Journal Geophysical Research*, *105*, 19477–19498.
- Duerr, A. E. S., & Dhanak, M. R. (2012). An assessment of the hydrokinetic energy resource of the Florida Current. *IEEE Journal of Oceanic Engineering*, *37*(2), 281–293.
- Edenhofer, O., & Kalkuhl, M. (2011). When do increasing carbon taxes accelerate global warming? A note on the green paradox. *Energy Policy*, *39*, 2208–2212.
- Finkl, C. W., & Charlier, R. (2009). Electrical power generation from ocean currents in the Straits of Florida: Some environmental considerations. *Renewable and Sustainable Energy Reviews*, *13*, 2597–2604.
- Garrett, C., & Cummins, P. (2007). The efficiency of a turbine in a tidal channel. *Journal of Fluid Mechanics*, *588*, 243–251.
- Garrett, C., & Cummins, P. (2008). Limits to tidal current power. *Renewable Energy*, *33*, 2485–2490.
- Hanson, H. P., Skemp, S. H., Alsenas, G. M., & Coley, C. E. (2010). Power from the Florida Current a new perspective on an old vision. *Bulletin of the American Meteorological Society*, *91*, 861–866.
- Hsin, Y.-C., Qiu, B., Chiang, T.-L., & Wu, C.-R. (2013). Seasonal to interannual variations in the intensity and central position of the surface Kuroshio east of Taiwan. *Journal Geophysical Research*, *118*, 4305–4316.
- Johns, W. E., Lee, T. N., Zhang, D., Zantopp, R., Liu, C.-T., & Yang, Y. (2001). The Kuroshio east of Taiwan: Moored transport observations from WOCE PCM-1 array. *Journal of Physical Oceanography*, *31*, 1031–1053.
- Kashino, Y., Espana, N., Syamsudin, F., Richards, K. J., Jensen, T., Dutrieux, P., et al. (2009). Observations of the North Equatorial Current, Mindanao Current, and the Kuroshio Current

- system during the 2006/07 El Niño and 2007/08 La Niña. *Journal of Oceanography*, 65, 325–333.
- Kawabe, M. (2005). Variations of the Kuroshio in the southern region of Japan: Conditions for large meander of the Kuroshio. *Journal of Oceanography*, 61, 529–537.
- Le Traon, P.-Y., Dibarboure, G., & Ducet, N. (2001). Use of a high-resolution model to analyze the mapping capabilities of multiple-altimeter missions. *Journal of Atmospheric and Oceanic Technology*, 18, 1277–1288.
- Lissaman, P. B. S. (1979). The Coriolis program. *Oceanus*, 22, 23–28.
- Lukas, R., Firing, E., Hacker, P., Richardson, P. L., Collins, C. A., Fine, R., et al. (1991). Observations of the Mindanao current during the western equatorial Pacific Ocean circulation study. *Journal Geophysical Research*, 96(C4), 7089–7104.
- Lumpkin, R., & Johnson, G. C. (2013). Global ocean surface velocities from drifters: Mean, variance, El Niño-Southern Oscillation response, and seasonal cycle. *Journal of Geophysical Research: Oceans*, 118(6), 2992–3006.
- Lutjeharms, J. R. E. (2006). *The Agulhas Current* (1st ed.). Berlin: Springer.
- Maximenko, N., Niiler, P., Centurioni, L., Rio, M.-H., Melnichenko, O., Chambers, D., et al. (2009). Mean dynamic topography of the ocean derived from satellite and drifting buoy data using three different techniques. *Journal of Atmospheric and Oceanic Technology*, 26(9), 1910–1919.
- Munk, W. H. (1950). On the wind-driven ocean circulation. *Journal of Meteorology*, 7, 79–93.
- Niiler, P. P. (2001). The world ocean surface circulation. *International Geophysics*, 77, 193–204. In G. Siedler, J. Church & J. Gould (Eds.), *Ocean circulation and climate: Observing and modeling the global ocean*. San Diego, Calif: Academic Press.
- Niiler, P. P., Sybrandy, A. S., Bi, K., Poulain, P. M., & Bitterman, D. (1995). Measurements of the water following capability of holey-sock and TRISTAR drifters. *Deep-Sea Research*, 42A, 1951–1964.
- Pascual, A., Faugere, Y., Larnicol, G., & Le Traon, P.-Y. (2006). Improved description of the ocean mesoscale variability by combining four satellite altimeters. *Geophysical Research Letters*, 33, L02611. doi:10.1029/2005GL024633.
- Ponta, F. L., & Jacovkis, P. M. (2008). Marine-current power generation by diffuser-augmented floating hydro-turbines. *Renewable Energy*, 33(4), 665–673.
- Poulain, P.-M., Gerin, R., Mauri, E., & Pennel, R. (2009). Wind effects on drogued and undrogued drifters in the eastern Mediterranean. *Journal of Atmospheric and Oceanic Technology*, 26, 1144–1156. doi:10.1175/2008JTECHO618.1.
- Qiu, B., & Chen, S. (2006). Decadal variability in the large-scale sea surface height field of the South Pacific Ocean: Observations and causes. *Journal of Physical Oceanography*, 36(9), 1751. doi:10.1175/JPO2943.1.
- Rio, M.-H., & Hernandez, F. (2004). A mean dynamic topography computed over the world ocean from altimetry, in situ measurements, and a geoid model. *Journal Geophysical Research*, 109, C12032. doi:10.1029/2003JC002226.
- Stommel, H. (1948). The westward intensification of wind-driven ocean currents. *Transactions American Geophysical Union*, 29, 202–206.
- Stramma, L., & Lutjeharms, J. (1997). The flow field of the subtropical gyre of the South Indian Ocean. *Journal Geophysical Research*, 99, 14053–14070.
- Twidell, J., & Weir, A. (2006). *Renewable energy resources*. Taylor and Francis.
- VanZwieten Jr., J. H., Duerr, A. E. S., Alsenas, G. M., & Hanson, H. P. (2013). Global ocean current energy assessment: An initial look. In *Proceedings of the 1st Marine Energy Technology Symposium (METS13)*, April 10–11, Washington D.C.
- VanZwieten, J. H., Meyer, I., & Alsenas, G. M. (2014). Evaluation of HYCOM as a tool for ocean current energy assessment. In *Proceedings of the 2nd Marine Energy Technology Symposium (METS14) April 15–18, 2014, Seattle, WA*.
- Yang, X., Haas, K. A., & Fritz, H. M. (2014). Evaluating the potential for energy extraction from turbines in the gulf stream system. *Renewable Energy*, 12–21.

- Yang, X., Haas, K. A., Fritz, H. M., French, S. P., Shi, X., Neary, V. S., et al. (2015a). National geodatabase of ocean current power resource in USA. *Renewable and Sustainable Energy Reviews*, 44, 496–507.
- Yang, Y. J., Jan, S., Chang, M.-H., Wang, J., Mensah, V., Kuo, T.-H., et al. (2015b). Mean structure and fluctuations of the Kuroshio east of Taiwan from in-situ and remote observations. *Oceanography*, 28(4), 74–83.
- Yang, Z., Wang, T., & Copping, A. E. (2013). Modeling tidal stream energy extraction and its effects on transport processes in a tidal channel and bay system using a three-dimensional coastal ocean model. *Renewable Energy*, 50, 605–613.